Supporting information

Direct Growth of Ultra-Permeable Molecularly Thin Porous Graphene Membranes for Water Treatment

Gaoliang Wei, Xie Quan, Chao Li, Shuo Chen, and Hongtao Yu

Membrane Performance Tests. Flux measurement and filtration tests were all performed using a dead-end membrane filtration system. Water permeance (P) of the ultrathin graphene membranes were measured at ambient temperature and calculated based on following equation:

$$P = \frac{V}{St\Delta p} \quad (1)$$

Where V is the volume of ultrapure water penetrating the membrane at a given time interval t, S is the effective area (1.0 cm×1.0 cm in this work) of porous graphene/polycarbonate membrane, Δp is the transmembrane pressure difference.

To characterize the recalcitrance to irreversible fouling of ultrathin graphene membranes, both polystyrene (PS) nano/microparticles with various diameters (10, 35, 60, 89 and 190 nm, 0.05wt%) and humic acid molecules (10 mg L^{-1}) were chosen as model pollutants in water. Conventional polyvinylidene fluoride (PVDF) ultrafiltration membranes were also investigated for comparison. Their flux recoveries (R) were calculated using following equation:

$$R = \frac{J}{J_0} \quad (2)$$

Where J is the flux after washing and J_0 is the initial flux of the membrane.

Preparation of PVDF Membranes. At 60 °C, 3.0 g Poly (vinyl pyrrolidone) (K30) and 3.0 g PVDF powders were dissolved in 14 g *N*, *N*-dimethylformamide to form a homogeneous viscous solution. Then a layer of the solution with a thickness of 100 μm was made on glass plate using a scraper, followed by being immerged in water for 1 h. After several washes, the obtained PVDF membranes was preserved in water before usage.

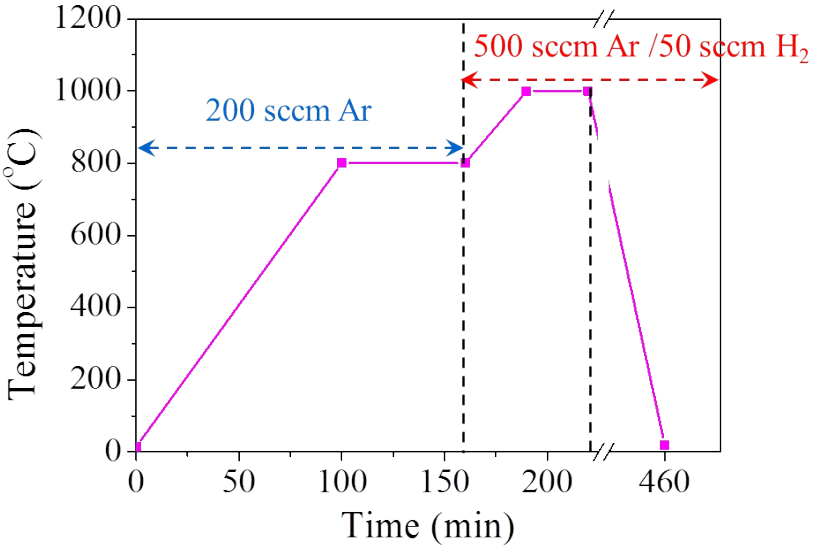

Fig. S1 Time dependence of experimental parameters: temperature and gas composition/flow rate.

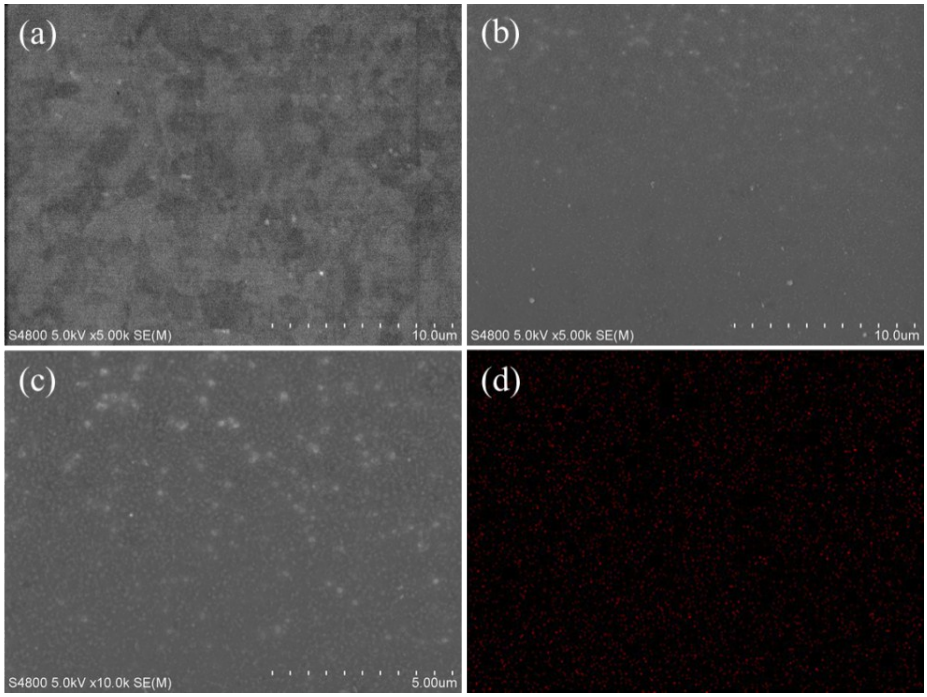

Fig. S2 (a) SEM image of Cu foil with a size of 1.5 cm×1.5 cm used in this work. (b) SEM image of Cu foil with a $Cu(NO_3)_2$/PMMA layer on it. (c) Magnified SEM image of $Cu(NO_3)_2$/PMMA/Cu foil sample. (d) Distribution of element N of the sample in (c).

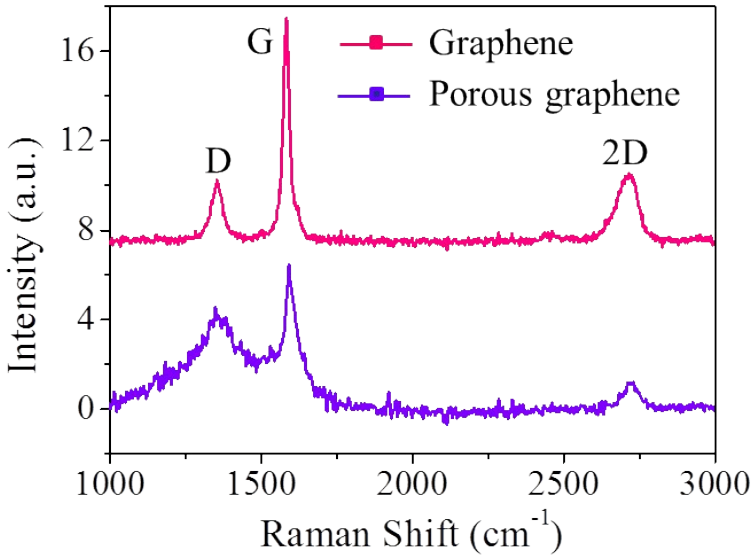

Fig. S3 Raman spectra of porous graphene and graphene sheets obtained by thermal conversion of PMMA on Cu foil.

In Fig. S3, two strong peaks centered at 1590 cm^{-1} (G band) and 2684 cm^{-1} (2D band), the typical characteristic peaks of graphene,[1] can be obviously observed, which suggests that porous graphene is successfully obtained by thermal conversion of PMMA on Cu

foil. Additionally, the Raman spectrum of pore-free graphene sheet fabricated with the same process without adding $Cu(NO_3)_2$ is also recorded. As revealed, its intensity ratio of D peak (1350 cm^{-1}, a characteristic of defects in the graphene) to G peak (I_D/I_G=0.26) is lower than that of porous graphene (I_D/I_G=0.65), which may be attributed to pore-induced more edges.

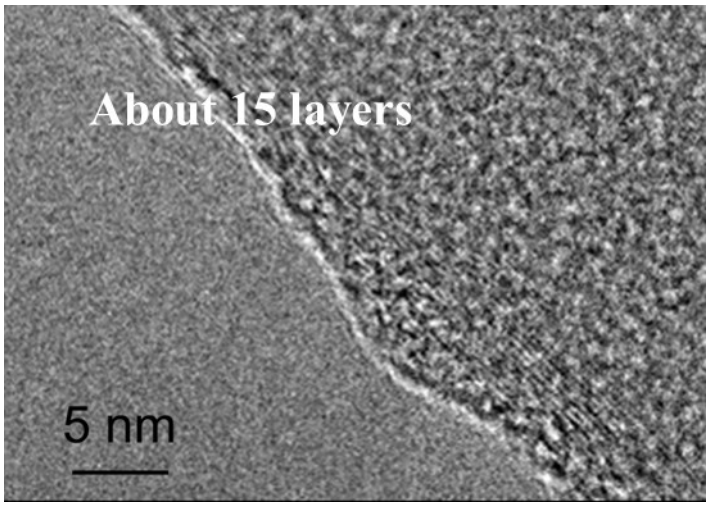

Fig. S4 High-resolution TEM image of the edge of porous graphene.

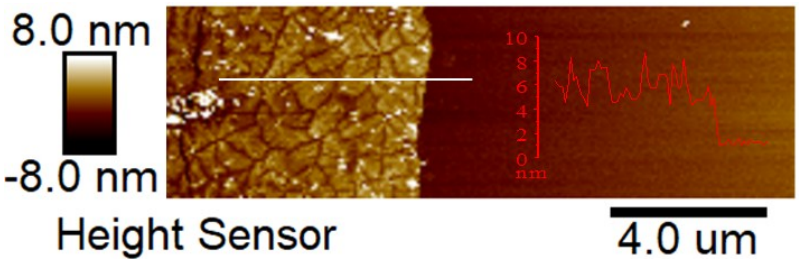

Fig. S5 AFM image of a porous graphene sheet transferred onto a mica substrate.

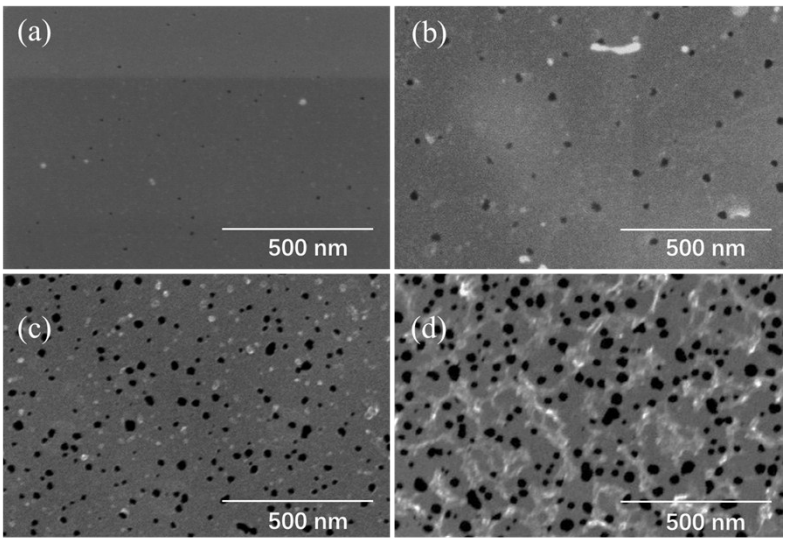

Fig. S6 SEM images of porous graphene membranes obtained at various $Cu(NO_3)_2$ concentrations: (a) 1.0, (b) 2.0, (c) 5.0 and (d) 10.0 g L^{-1}.

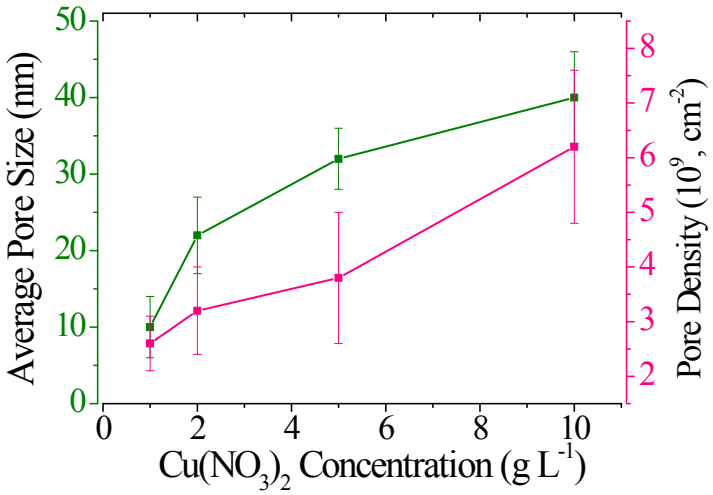

Fig. S7 Average pore size and pore density as a function of $Cu(NO_3)_2$ concentration in acetone.

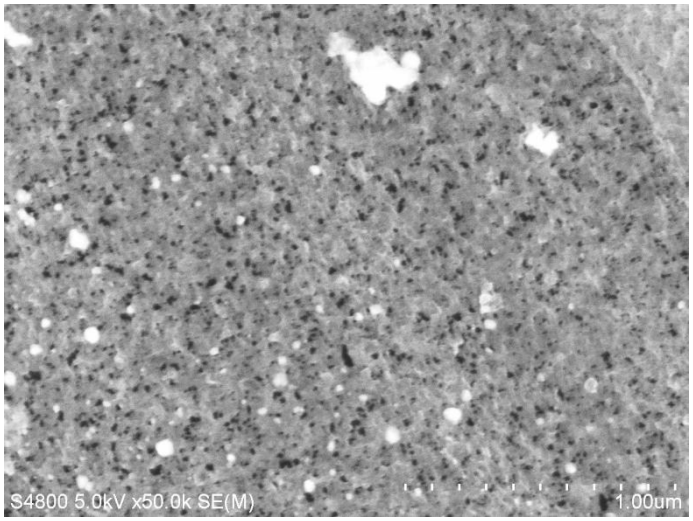

Fig. S8 SEM image of a sample obtained at a $Cu(NO_3)_2$ concentration of 20.0 g L^{-1}.

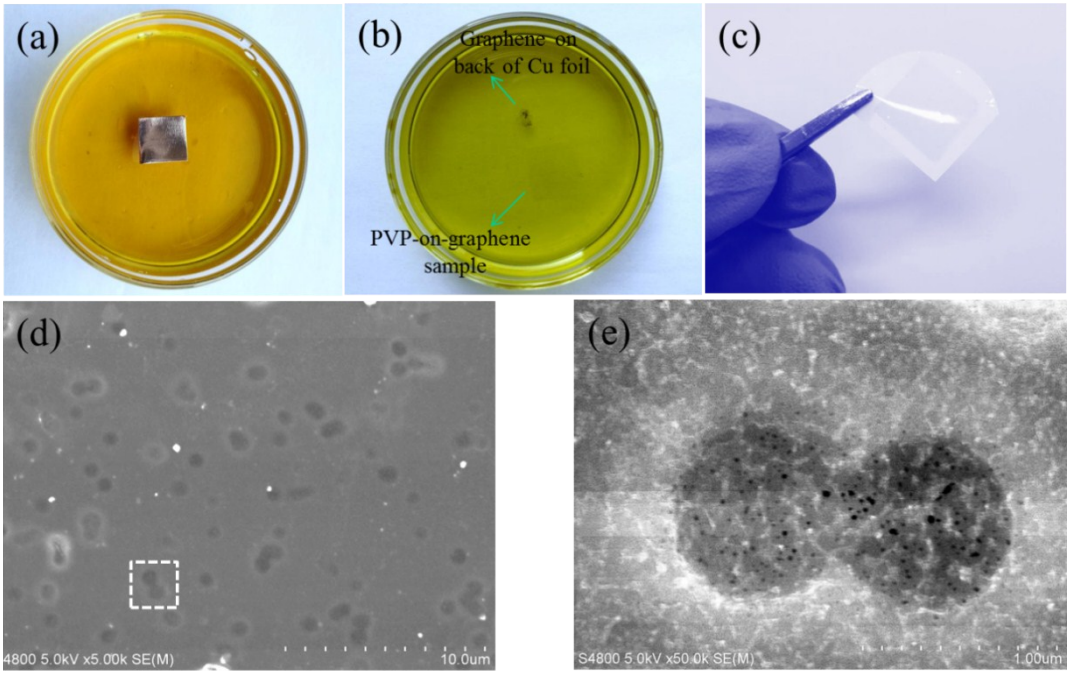

Fig. S9 (a) A PVB/Cu nanoparticle/graphene/Cu foil sample is floating on $FeCl_3$/HCl solution. (b) The sample in (a) after removal of Cu foil and Cu nanoparticles. (c) The sample in (b) after being transferred on a porous polycarbonate substrate. (d) SEM image of a porous graphene-on-polycarbonate sample. (e) Magnified SEM image of the area marked in white rectangle in (d).

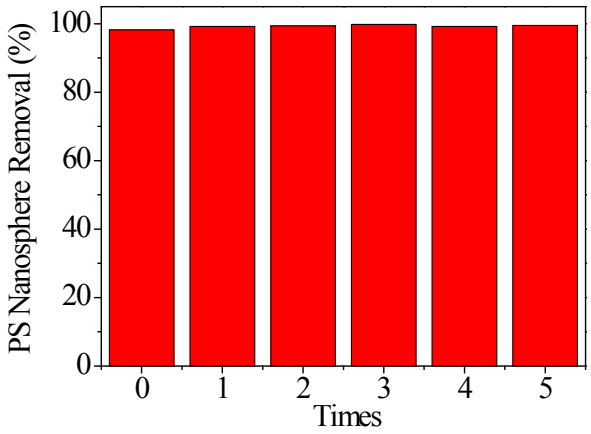

Fig. S10 Removal rate of PS nanospheres by graphene membranes as a function of back-flush times.

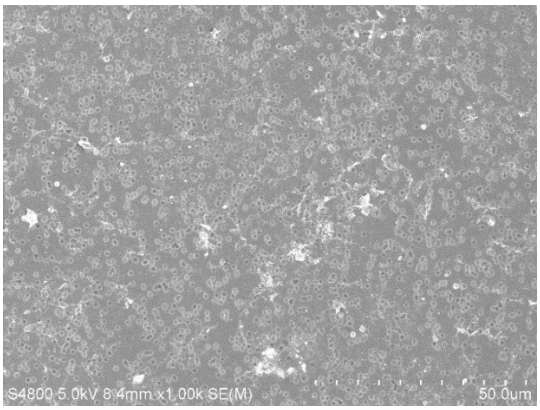

Fig. S11 SEM image of graphene/polycarbonate membrane after back flushes.

To remove PVB molecules on graphene membrane, the as-prepared samples are immerged in ethanol for several hours. Thus, a little of PVB molecules dissolved in ethanol will transfer to the junction of graphene and polycarbonate support, where it can function as glue to stick them together after drying. Due to the mechanical adhesion and Van der Waals' force, the porous graphene skin-layer can thus survive from water pressure, even in the back-flush mode. To evidence the structural integrity of graphene membrane after tests, the removal rates (%) of 60 nm PS nanospheres are analyzed. As shown in Fig. S10, all removal rates are still nearly 100% after back flushes, which is higher than ~98% of as-prepared membranes. These results suggest there are no structural fractures in graphene membrane after back flushes. The SEM image shown in Fig. S11 also reveals a crack-free graphene film, further confirming good mechanical strength and adhesion of graphene membrane with polycarbonate support.

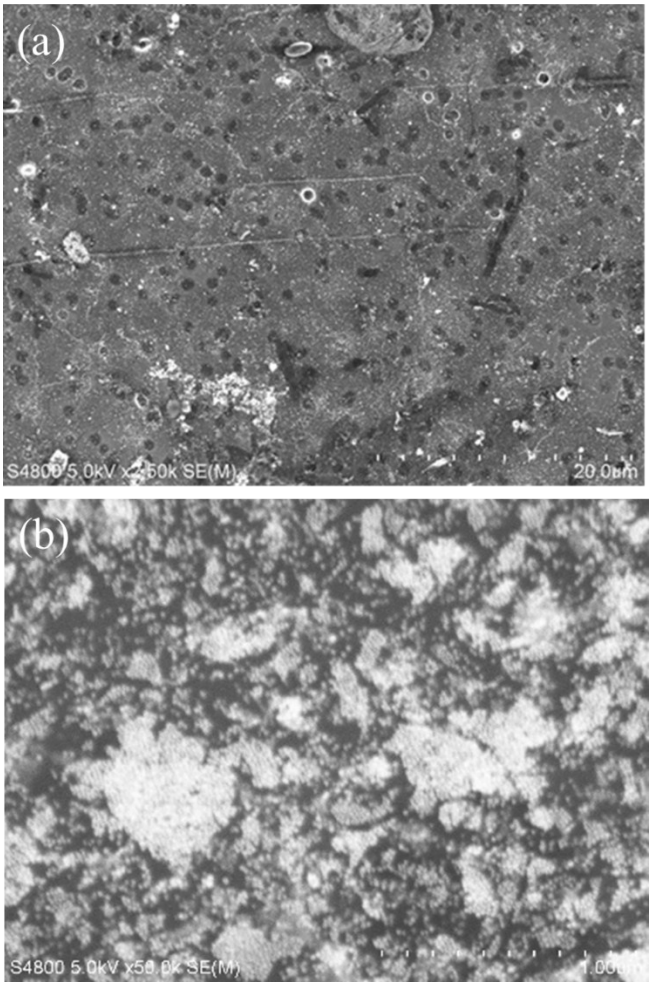

Fig. S12 (a) Low-resolution and (b) high-resolution SEM images of graphene membrane after filtration of 35 nm PS nanoparticles.

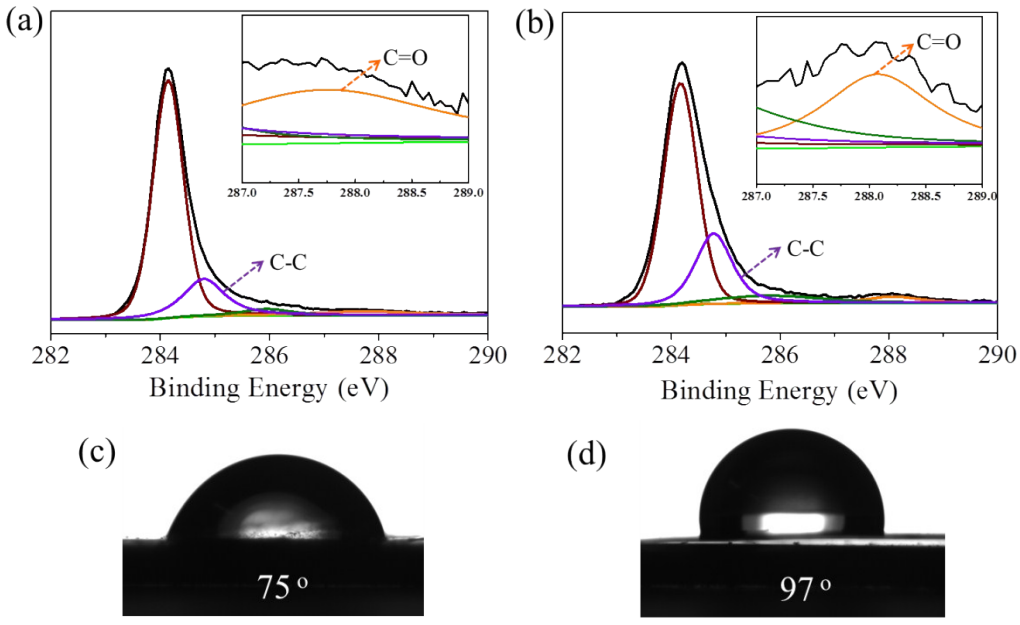

Fig. S13 (a) XPS analysis of pore-free graphene. (b) XPS analysis of porous graphene

membrane. (c) Water contact angle on porous graphene membrane. (d) Water contact angle on pore-free graphene.

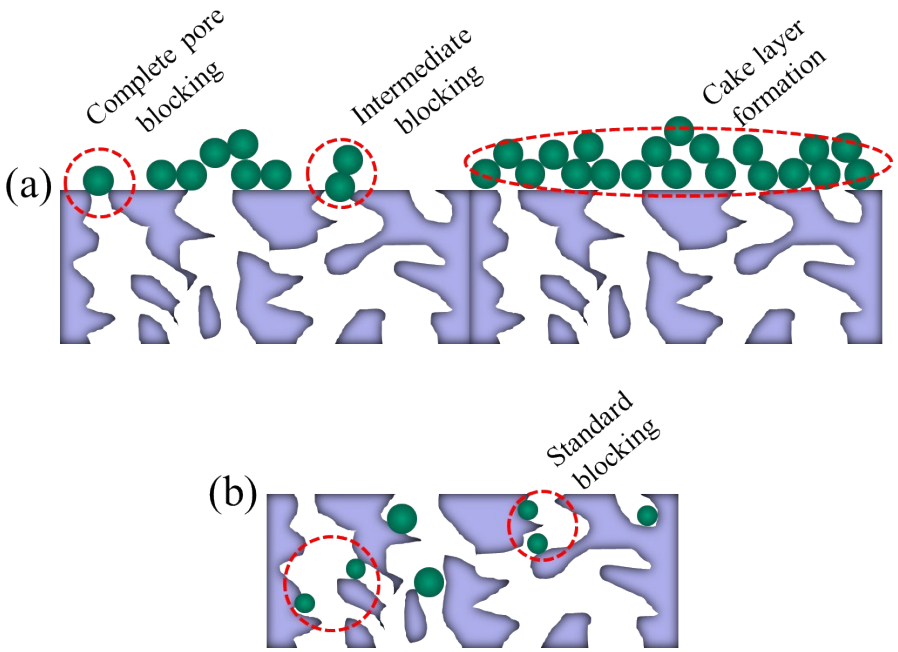

Fig. S14 Schematic representation of blocking mechanisms: (a) fouling on membrane surface; (b) fouling in pore channels.

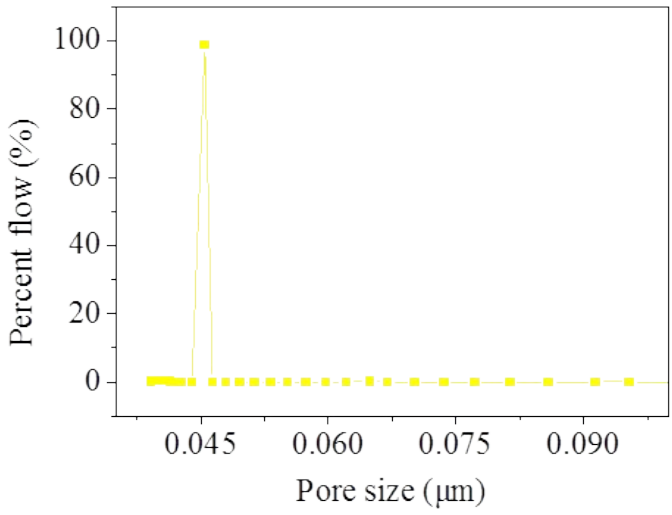

Fig. S15 Pore size distribution of PVDF membranes measured by a pore size analyzer (Porolux 1000, IB-FT GmbH, Germany).

Reference:

(1) Malard, L. M.; Pimenta, M. A.; Dresselhaus, G.; Dresselhaus, M. S. Raman spectroscopy in graphene. *Phys. Rep.* **2009**, *473*, 51-87.